

# Synthesis and Characterization of White-Emitting CdS Quantum Dots Stabilized with Polyethylenimine

Oleksandra E. Rayevska,<sup>†</sup> Galyna Ya. Grodzyuk,<sup>†</sup> Volodymyr M. Dzhagan,<sup>\*,‡</sup>  
Oleksandr L. Stroyuk,<sup>\*,†</sup> Stepan Ya. Kuchmiy,<sup>†</sup> Victor F. Plyusnin,<sup>§,||</sup> Vyacheslav P. Grivin,<sup>§</sup>  
and Mykhailo Ya. Valakh<sup>‡</sup>

*Pysarzhevskiy Institute of Physical Chemistry of National Academy of Sciences of Ukraine, Kyiv, Ukraine, Lashkaryov Institute of Semiconductor Physics of National Academy of Sciences of Ukraine, Kyiv, Ukraine, Institute of Chemical Kinetics and Combustion of Siberian Branch of Russian Academy of Sciences, Novosibirsk, Russian Federation, and Novosibirsk State University, Novosibirsk, Russian Federation*

*Received: September 8, 2010; Revised Manuscript Received: November 9, 2010*

We report on the synthesis and optical and structural characterization of ultrasmall (<2 nm) CdS nanoparticles with a narrow size distribution of 10% prepared in aqueous and alcohol solutions of polyethylenimine (PEI). The PEI-stabilized CdS nanoparticles reveal a structured absorption band with the first excitonic maximum at 3.5 eV and broad-band photoluminescence with quantum yields of 12–14% in water, 18–20% in ethanol (80 vol %), and up to 60–70% in solid PEI films at room temperature. The nature of the photoluminescence was studied by using the time- and wavelength-dependent emission measurements. The role of precursor cadmium(II)–PEI complex in the formation of uniform and ultrasmall luminescent CdS nanoparticles, as well as the dynamic emission quenching by water, are discussed. A study of the photochemical properties of PEI-stabilized CdS nanoparticles both under continuous and nanosecond pulse illumination showed excellent stability of solid PEI films incorporating CdS nanoparticles toward UV illumination and reductive character of the CdS nanoparticle photocorrosion in aqueous solutions.

## Introduction

Ultrasmall semiconductor nanoparticles or quantum dots (QDs), with a diameter of less than 2 nm, have become a recent topic of intense investigations.<sup>1–5</sup> First, the interest is driven by their inherent broad photoluminescence (PL) spectrum, promising for applications in the white-light emitting devices.<sup>1,5,6</sup> Furthermore, the nanoparticles of such a small size are attractive as luminescent markers for those bio- and medical applications where the nanoparticle size is a critical parameter concerning the penetration of the functionalized QDs through the cell walls.<sup>7</sup> In this connection, the application–attractive composites of ultrasmall nanoparticles with different kinds of biocompatible polymers (polyelectrolytes, block-copolymers, dendrimers, etc.) have been studied.<sup>8–12</sup> The conjugation of QDs with biofriendly polymers is of particular significance, as it allows one to avoid the loss of PL intensity at the stage of ligand exchange and transfer from organic to aqueous media.<sup>7,13,14</sup> The direct synthesis of water-soluble polymer-capped ultrasmall nanoparticles with reasonably high PL quantum yields still remains a challenge to be addressed. Finally, in the case of ultrasmall QDs, the study of fundamental physical and chemical properties of inorganic semiconductors under the regime of very strong exciton confinement becomes possible, involving simultaneously both the solid state and the molecular approaches.

Here, we report on synthesis and optical and structural characterization of ultrasmall CdS QDs prepared in aqueous and alcohol solutions of polyethylenimines. The polyethylenimine (PEI) is known to be a polyelectrolyte applicable in fabrication of thin-film QD-based light-emitting devices,<sup>15</sup> as well as an effective transfection agent in the intracellular DNA and genes delivery.<sup>7</sup> Even though it was observed previously<sup>16</sup> that the addition of PEI to the solution with CdS QDs stabilized with mercaptoacetic acid remarkably increases the intensity of the broad-band PL, the rare attempts to synthesize CdS nanoparticles directly in solutions of hyperbranched PEI did not give comparable PL output.<sup>8,9</sup> In contrast to these previous reports, in this work the highly luminescent (with the quantum yields up to 60–70% at room temperature) CdS QDs with a broad (white-like) emission have been synthesized directly in the solution of PEI used as both the stabilizing and the surface-passivating agent. A study of the dependence of the PL line shape, intensity, and lifetime on the synthesis conditions, aimed at understanding the origin of the strong PL emission and capabilities of its application, is reported.

## Materials and Methods

Cadmium chloride, Na<sub>2</sub>S × 9H<sub>2</sub>O, and polyethylenimine (50 wt % aqueous solution, *M<sub>w</sub>* = 2000, 50 000, and 750 000) were purchased from Sigma Aldrich and used without further purification.

The colloidal cadmium sulfide QDs were synthesized in a reaction between Cd<sup>2+</sup> and HS<sup>−</sup> in the presence of PEI in water and water/ethanol mixtures. In a typical procedure, 1 mL of 0.2 M CdCl<sub>2</sub> solution was added to 18 mL of 0.25 wt % PEI solution. To the resulting viscous solution was added 1 mL of 0.2 M Na<sub>2</sub>S solution under vigorous stirring.

\* Corresponding author. Tel./fax: +380 (44) 525-0270. E-mail: stroyuk@inphyschem-nas.kiev.ua, alstroyuk@ukr.net.

<sup>†</sup> Pysarzhevskiy Institute of Physical Chemistry of National Academy of Sciences of Ukraine.

<sup>‡</sup> Lashkaryov Institute of Semiconductor Physics of National Academy of Sciences of Ukraine.

<sup>§</sup> Siberian Branch of Russian Academy of Sciences.

<sup>||</sup> Novosibirsk State University.

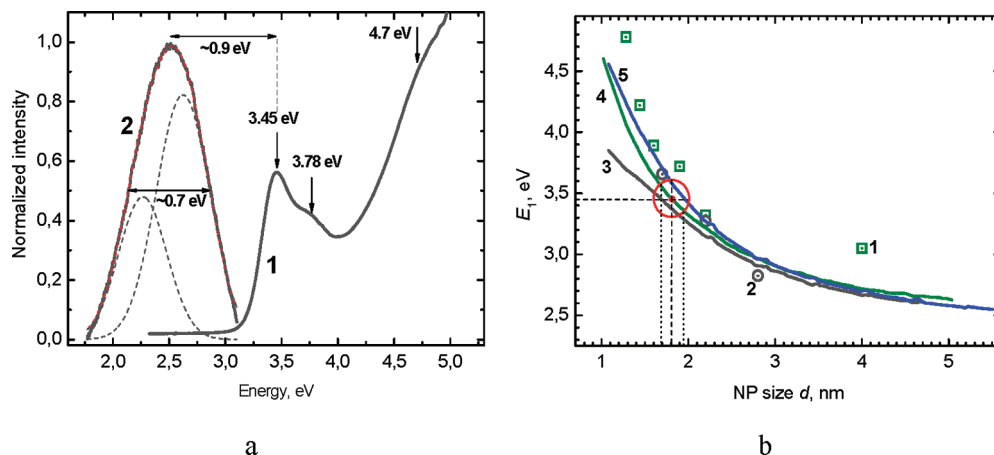


**Figure 1.** (a) Normalized typical absorbance (curve 1) and PL (curve 2) spectra of colloidal PEI-stabilized CdS QDs in water. Dash lines: A two-Gaussian deconvolution of the PL spectrum. (b) The  $E_1$  versus  $d$  dependences for CdS nanoparticles derived from the experimental data and semiempirical models. The squares (curve 1) represent the data of ref 20, circles ref 21, curves 3,5 ref 22, and curve 4 ref 23. The red circle defines the size distribution derived from the fwhm of  $E_1$  peak.

To prepare the films of PEI-stabilized CdS nanoparticles, 2 mL of 0.1 M CdS solutions with 2.5 wt % PEI was deposited onto previously cleaned  $2 \times 2$  cm glass or quartz substrates and left drying at natural ventilation in the dark.

The absorbance spectra were registered with a Specord 220 or an HP Agilent 8453 spectrophotometer. The photoluminescence spectra were taken on a Perkin-Elmer LS55 or Edinburgh Instruments FLS920 luminescence spectrometer. The luminescence decay profiles were obtained using an Edinburgh Instruments FLS920 photon counting system equipped with a EPL-375 ps diode laser emitting 60 ps pulses with  $\lambda = 375$  nm. The XRD spectra were registered using a DRON-3 M diffractometer with a copper  $K_\alpha$  irradiation source.

The laser flash photolysis experiments were carried out on an automated homemade setup equipped with a pulse Nd laser (third harmonic,  $\lambda = 355$  nm, 5 ns, 1–10 mJ). The laser pulse energy was measured using the ferrioxalate actinometer and the Gentec-EO (Canada) system (SOLO-2 monitor and pyroelectric measuring cap QE25SP-H-MB).

The stationary photolysis was carried out in air at ambient conditions in 10.0 mm optical quartz cuvettes (in case of solutions) using the light of a high-pressure mercury lamp equipped with a combination of optical filters cutting a narrow spectral region of 310–390 nm ( $5 \times 10^{18}$  quanta per min). The intensity of mercury lines was controlled by means of the Gentec-EO system with a photodiode measuring cap PH100-SiUV.

## Results and Discussion

As an introductory remark, it should be noted that PEI-stabilized cadmium sulfide QDs, although in some aspects being similar to the “conventional” colloidal CdS nanoparticles, generally reveal drastically different properties. Opposite to other types of colloidal CdS nanoparticles, stabilized by water-soluble organic polymers (gelatin or polyvinyl alcohol<sup>10</sup>), bulky inorganic ions (polyphosphate<sup>17</sup>), or ionic species ( $\text{Cd}^{2+}$ <sup>10,17</sup> or  $\text{S}^{2-}$ ), the PEI-stabilized CdS QDs manifest several orders of magnitude higher PL efficiency and achievable concentration of colloidal particles (up to 50% of CdS in terms of polymer mass can be introduced into PEI solution without any loss of stability and PL efficiency) as well as unusual for this size range narrow size distribution and aggregative stability.

Typical colloidal approaches to nanoparticle size variation (change in polymer concentration, aging, thermal coarsening,

introduction of an excess of  $\text{Cd}^{2+}$  or  $\text{S}^{2-}$ ) are not effective in the case of PEI-stabilized CdS QDs. Here, a narrow range of optimal concentration and ratio of cadmium(II), sulfur(II), and PEI exists where the most stable and luminescent QDs with a mean diameter as small as 1.8 nm and size distribution  $\sim 10\%$  can be produced. Beyond this range, pronounced deterioration of unique properties of PEI-stabilized CdS QDs is observed, indicating a special stabilization and surface passivation mechanism differing from that for other stabilizers.

**Absorbance Spectrum of CdS-PEI QDs.** The optical absorbance spectra of PEI-stabilized CdS QDs both in aqueous solutions and in water/ethanol mixtures reveal an absorption onset shifted to higher energies by 0.7–0.9 eV as compared to bulk cadmium sulfide with a distinct band structure just above the onset (Figure 1a). The lowest energy features,  $E_1$  at 3.45 eV and  $E_2$  at 3.78 eV, can be assigned to the  $1\text{S}_e-1\text{S}_{3/2}$  and  $1\text{S}_e-2\text{S}_{3/2}$  interband transitions, correspondingly.<sup>18,19</sup> The third feature at about 4.7 eV is also resolvable.

The absorbance spectra of cadmium sulfide nanoparticles are widely used to determine both their average size and their size dispersion.<sup>18,20–23</sup> This approach proceeded from the dependence of the first excitonic absorption peak position on the nanoparticle size  $d$ . A number of calibration curves were derived for such dependence, both empirically<sup>18</sup> and from calculations.<sup>20–23</sup> The scatter of the reported data is, however, extremely large ( $>50\%$ ) in the range of  $E_1 > 3.1$  eV. The fact may be accounted for, first, by a very steep  $E_1(d)$  dependence in this spectral range and, second, due to a noticeable influence of the ligand (stabilizer) and solvent onto the electronic structure of such ultrasmall nanoparticles.<sup>4,20,21,24–26</sup>

Estimations of the average size of PEI-stabilized CdS QDs reported here were based mainly on the data reported in refs 18, 20–23, which show the least contradiction one with another (Figure 1b). Using Figure 1b and fitting  $E_1$  peak position in the absorbance spectra (Figure 1a), the average size was estimated as  $d = 1.8 \pm 0.1$  nm for the PEI-stabilized colloidal CdS QDs. The spectral width (fwhm) of the  $E_1$  peak,  $\Gamma_{E_1} = 0.3$  eV, corresponds to a size distribution of  $\sim 10\%$  (red circle in Figure 1b).

Typically, the average size of polymer-stabilized colloidal CdS nanoparticles is reduced with decreasing the concentration of precursors (cadmium and sulfide salts).<sup>10,17,27</sup> This is not the case for the PEI-stabilized CdS QDs revealing an optimal range of cadmium sulfide concentration where both the average size

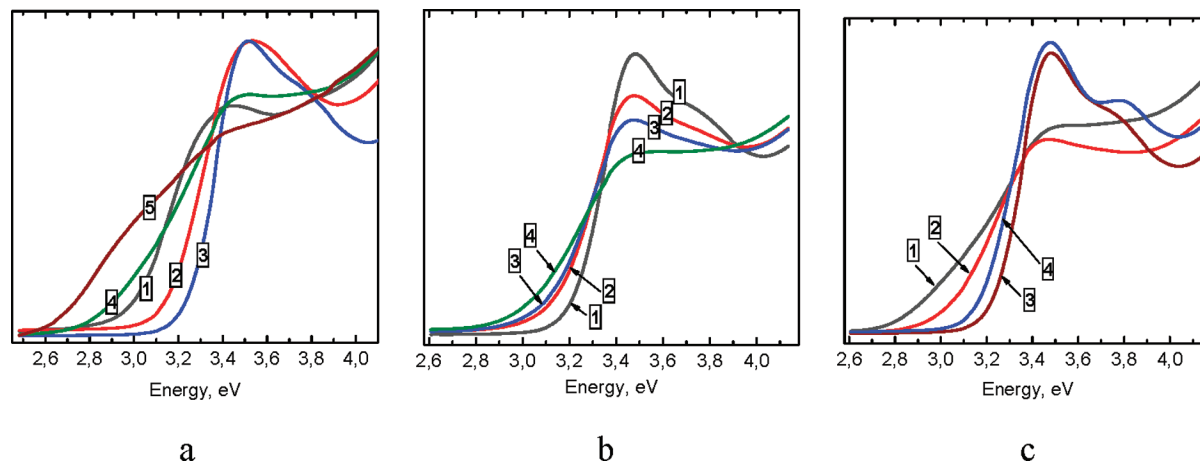


**Figure 2.** Normalized absorbance spectra of aqueous PEI-stabilized CdS QDs synthesized (a) at different cadmium sulfide concentration:  $5 \times 10^{-4}$  (curve 1),  $2 \times 10^{-3}$  (curve 2),  $1 \times 10^{-2}$  (curve 3),  $2 \times 10^{-2}$  (curve 4), and  $4 \times 10^{-2}$  M (curve 5); (b) at cadmium sulfide concentration of  $1 \times 10^{-2}$  M with the stoichiometric ratio of  $\text{Cd}^{2+}$  and  $\text{S}^{2-}$  (curve 1) and with a  $\text{Cd}^{2+}$  excess of 20% (curve 2), 50% (curve 3), and 100% (curve 4), 0.25% PEI; and (c) at  $[\text{CdS}] = 1 \times 10^{-2}$  M with different PEI content –0.10% (curve 1), 0.25% (curve 2), 2.50% (curve 3), and 5.00% (curve 4).

and the size dispersion of QDs are minimal. Figure 2a shows that at 0.25 wt % PEI the optimal  $\text{Cd}^{2+}$  concentration is around  $1 \times 10^{-2}$  M. Taking into account that the elementary PEI unit  $-\text{CH}_2\text{CH}_2\text{NH}-$  has a mass of 43 g per mole, this solution composition corresponds to around 1 Cd atom per 6 N atoms.

Studies of cadmium(II) sorption from water by the PEI membranes<sup>28</sup> showed that the maximal membrane capacitance in terms of  $\text{Cd}^{2+}$  also corresponds to  $\text{Cd}:\text{N} = 1:6$ , indicating a complete saturation of coordination sphere of cadmium(II) ions with amino groups. Formation of the same saturated complex can account for the optimal  $\text{Cd}^{2+}$  concentration range in the system discussed here. A number of experimental facts supporting this assumption were collected.

(1) The properties of PEI-stabilized CdS QDs are the same at different CdS and PEI content provided the optimal ratio of  $\text{Cd}:\text{N} = 1:6$  is maintained. For example, the average size and optical properties of CdS QDs prepared at  $[\text{CdS}] = 0.01$  M and 0.25% PEI and  $[\text{CdS}] = 0.1$  M and 2.5% PEI are identical. In this way, the molar concentration of PEI-stabilized CdS QDs can be increased up to 0.2 M without noticeable deterioration of absorption and PL properties.

(2) Opposite to conventional aqueous syntheses of CdS nanoparticles, where introduction of an excess of  $\text{Cd}^{2+}$  or  $\text{S}^{2-}$ , and, to some extent, increase in polymer concentration normally results in a decrease of the average nanoparticle size,<sup>10,17</sup> in the case of PEI-stabilized CdS QDs any deviation from an optimal Cd:S ratio by adding the  $\text{Cd}^{2+}$  excess (Figure 2b) or from an optimal CdS:PEI ratio by increasing the polyelectrolyte concentration (Figure 2c) results in the QD size increase and defocusing of the size distribution. No special dependences between the optical properties of PEI-stabilized CdS QDs and the molecular mass of the polymer were found; the CdS QDs stabilized by PEI with  $M_w = 2000$  g/mol were unstable, while increasing  $M_w$  from 50 000 to 750 000 did not change appreciably the stability, absorbance, and PL characteristics of QDs.

(3) pH of aqueous PEI solution decreases upon titration with cadmium chloride, indicating formation of a complex between amino groups and  $\text{Cd}^{2+}$  (see the Supporting Information, Figure S1a). At that, deprotonation of  $-\text{NH}_2^+-$  groups occurs due to the complexation with cadmium, which results in recombination of released protons with  $\text{OH}^-$  anions and the observed pH reduction. Figure S1a shows that 99.9% of starting  $\text{OH}^-$  ions are consumed at the ratio  $\text{Cd}:\text{N}$  of around 1:6.

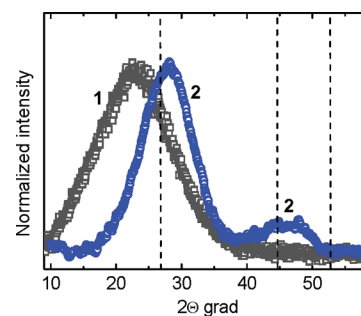


**Figure 3.** Normalized X-ray patterns from pure PEI ( $\square$ , curve 1) and CdS-PEI films (blue  $\circ$ , curve 2). The position of reflexes for the bulk cubic CdS is marked by the dashed lines.

(4) A strong increase in viscosity is observed upon  $\text{CdCl}_2$  addition to PEI solutions. The fact can be the indication of interlinking of the polymer chains probably by simultaneous coordination of  $-\text{NH}-$  groups of several polyelectrolyte chains to each  $\text{Cd}^{2+}$  ion. At that, a regular three-dimensional network of 6-coordinated Cd atoms can form, providing favorable conditions for the formation of uniform and ultrasmall CdS nanoparticles tightly surface-passivated with amino groups.

The XRD pattern of PEI-stabilized CdS QDs (Figure 3) shows two broad diffraction peaks, from which it is not possible to distinguish between wurtzite and zinc blend structures, as was previously observed for the ultrasmall CdS,<sup>26</sup> CdSe,<sup>4,29,30</sup> and CdTe nanoparticles.<sup>31</sup> Similar wide-angle XRD patterns were reported in ref 20 for 1.8–2.4 nm CdS QDs as determined independently by TEM and small angle XRD. On the basis of the X-ray pattern of PEI-stabilized CdS QDs, one can at least conclude that they are rather crystalline than amorphous. For the amorphous phase, a single and very broad peak is expected around the position of (111) peak, similarly to the X-ray pattern of PEI (Figure 3, curve 1). Moreover, the upward shift of the main reflex up to  $27.7^\circ$  may be the indication of Cd–S bond contraction in CdS QDs, as compared to the bulk cadmium sulfide, in correspondence with the results of ref 26 for 1.5 nm CdS nanoparticles.

The attempts to probe the size or structure of PEI-stabilized CdS QDs by HRTEM gave no meaningful results. Only blurred nanoaggregates of nondistinct 3–4 nm particles with no detectable crystalline fringes were observed (Supporting Information, Figure S2). Probably, the large size of aggregates as compared to the size of individual QDs and especially the

charging of PEI molecules under the electron beam precludes the ultrasmall CdS nanoparticles to be distinguished separately.

Much more informative appeared the characterization of CdS-PEI QDs using atomic force microscopy (Supporting Information, Figure S3). It can be seen from Figure S3a,c that the polyethyleneimine forms a smooth layer on the surface of a silicon substrate with the average roughness as small as 0.2 nm. The CdS-PEI, on the contrary, exhibits much more pronounced roughness, which is 1.8–2.0 nm (Figure S3b,d), that is close to the estimations of the CdS QDs size derived from the optical measurements. From Figure S3b,d follows also that there are virtually no QDs larger than 2.2–2.3 nm, which confirms the above estimations of the size distribution made from the spectral width of the first two excitonic maxima in the absorbance spectra.

As discussed, the XRD and HRTEM studies of PEI-stabilized CdS QDs did not produce reliable values of nanoparticle size. Therefore, in the following discussion, the value of  $1.8 \pm 0.1$  nm derived from the optical absorbance data is adopted. However, this value probably should be regarded as an estimate not only because of the uncertainties of the experimental data and calibration curves reported (Figure 1b), but also due to the more or less strong influence of surrounding media (specifically, electron density of a passivating agent, type of surface termination, etc.) on the exciton confinement and optical properties of ultrasmall ( $d < 3$  nm) semiconductor nanoparticles. For example, the first excitonic maximum of a “magic” cluster  $\text{Cd}_{32}\text{S}_{14}\text{L}_{36}$  with the core size of 1.7 nm (L = passivating ligand) was reported to shift from 325 nm for L =  $\text{SCH}_2\text{CH}(\text{OH})\text{CH}_3$ <sup>21,32</sup> to 358 nm for the aromatic ligand L =  $\text{SC}_6\text{H}_5$ ,<sup>21,25</sup> the fact tentatively attributed to the interaction of the exciton with the aromatic thiophenolate rings resulting in a reduced spatial exciton confinement.

Binding of  $\text{NH}_2$  groups to  $(\text{CdSe})_6$  cluster has been predicted to increase the HOMO–LUMO transition energy of  $(\text{CdSe})_6$ <sup>33</sup> and a series of larger cadmium selenide clusters<sup>34</sup> by  $\sim 0.1$  eV per structural unit. Even though the amino-group influence onto the gap energy of the present larger CdS-PEI QDs (with many internal atoms not bound to amine groups) may be not as strong as for the small cluster with each Cd atom bound to amine, this effect is obviously to be kept in mind at estimation of the nanoparticle size from the absorption spectra.

The authors of ref 25 demonstrated a reversible adsorption-enhanced quantum confinement in semiconductor QDs via adsorption/desorption of the cyanide. The negative charge of  $\text{CN}^-$  (similarly to the unbound electron pair of nitrogen atoms in  $-\text{NH}-$  groups of PEI) on the surface compresses the electron wave function in the QD, with the resulting strongly size-dependent absorption shift reaching as much as 250 meV for 3.5 nm particles.<sup>25</sup> Obviously, even when other adsorbates or surfactants have a weaker effect, it can be still noticeable for CdS nanoparticles as small as 1.5–2.0 nm, introducing uncertainties in the determination of nanoparticle size from the position of the first absorption maximum, as the calibration curves used were established for CdS nanoparticles with completely different ligands and surrounding media.

**Photoluminescence of CdS-PEI QDs.** The PEI-stabilized colloidal CdS QDs reveal a broad ( $\Gamma_{\text{PL}} \approx 0.5$  eV) PL band in the region of 2–3 eV with a nondistinct maximum at 2.45–2.65 eV (Figure 1a). The band is shifted by 0.5 eV from the absorption onset and by 0.9 eV from the first excitonic maximum. The PL band of PEI-stabilized CdS QDs typically has a complex shape depending upon the synthesis conditions

and excitation wavelength (Supporting Information, Figure S4) and can be deconvoluted into 2–3 Gaussian profiles (Figure 1a).

The PL spectra of the kind are normally assigned to the radiative electron–hole recombination with one (or both) charge carriers localized by a “deep trap”.<sup>27,35</sup> One of the approaches, most frequently used to explain the large width of deep-trap PL band in both nano- and macrocrystals, is the distance distribution of the donor–acceptor (D–A) pairs, with the larger emission energies (shorter wavelengths) corresponding to shorter distances.<sup>35</sup> From the simple considerations, the range of D–A pair distances is significantly reduced in the nanoparticles as small as 1.8 nm. However, the deep-trap PL band remains as broad as for larger nanoparticles and for bulk crystals, where the range of possible D–A distances can be obviously wider. The D–A model can be the right one, however, when we assume that the range of D–A distances, which have high enough recombination probability to appear in the PL spectrum, is roughly the same for nano- and macrocrystals, and limited to several shortest distances. The time-resolved PL measurements of CdS-PEI QDs, reported below, show the PL rate growing with the increase of quantum energy, which is in qualitative accordance with the D–A– pair recombination model.<sup>27,35</sup>

A strong coupling of the exciton with the surface/interface vibrations has been intensively discussed for Si nanoparticles in oxide matrix, and the coupling of the exciton to the Si–O vibration at the interface nanoparticle–matrix has been demonstrated to play a determinant role in the recombination processes.<sup>36,37</sup> The underlying exciton–phonon coupling via Frölich mechanism can be much stronger in II–VI nanoparticles and manifests itself most strongly in the small nanoparticles with a large number of surface atoms. In other words, for nanoparticles as small as several CdS interplanar distances, the strong localization of electronic and lattice excitations can result in a high probability of phonon emission during electronic relaxation.<sup>38</sup> The apparent PL line shape may thus be a superposition of several bands due to emission from different electronic states, broadened by the strong coupling of the deeply trapped electron with the lattice vibrations. Indeed, there are reports in the literature that demonstrate a strong coupling to phonons of the strongly localized excitation.<sup>38</sup> The size dispersion of PEI-stabilized CdS QDs, although as small as 10%, can also contribute to the complex shape of the PL spectra, as we probe a fraction of larger QDs by lowering the excitation energy (Figure S4b).

In view of the picture of a nonhomogenous structural relaxation over nanoparticle volume,<sup>39</sup> one may assume that for the very small CdS-PEI nanoparticles the PL band position and width are due to emission of the exciton localized to the outer (surface) region, the most energetically favorable region of the QD. The gap states, corresponding to these relaxed regions, have obviously very weak oscillator strength in absorption, and thus the absorption is dominated with sharp features corresponding to the exciton generated in the (bulk) “core” of the QD. For the emission, in contrast, there may be a strongly concurrent route of exciton to be localized with the outer (surface) region of the QD before recombination. Therefore, the relative probabilities of the exciton to radiatively recombine in the “core” or from the trapped state will obviously determine whether we observe excitonic band or only broadened and red-shifted trap-state emission. In this case, not only the nanoparticle size is determinant but also the “actual” localization diameter of the exciton, determined also by ligands, as discussed above.

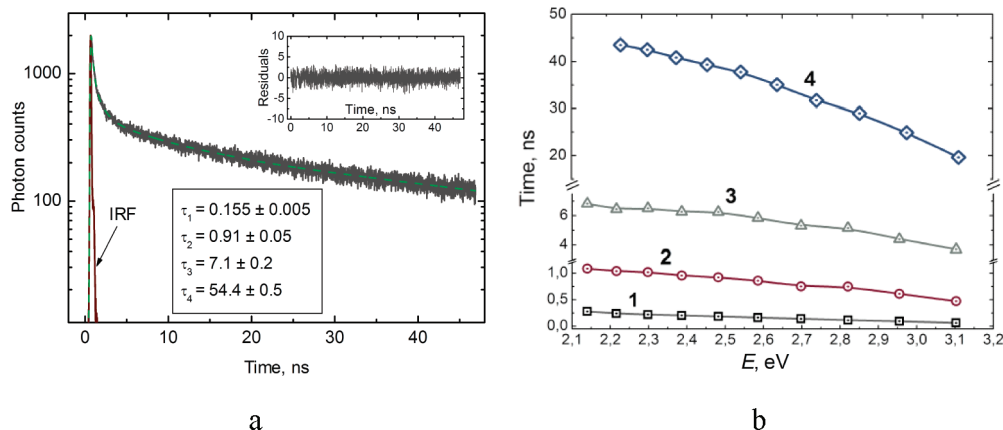


**Figure 4.** (a) PL decay profile registered at 500 nm for CdS QDs incorporated in a PEI film. Dashed line is a four-exponent fit of the decay profile,  $\tau_1$ ... $\tau_4$  are time constants derived from the fitting, and IRF is the instrumental response function. Inset: Residuals after the four-exponential fitting of the decay profile. (b) Wavelength dependence of time constants  $\tau_1$  (curve 1),  $\tau_2$  (curve 2),  $\tau_3$  (curve 3), and  $\tau_4$  (curve 4).

**PL Decay Dynamics.** The time-resolved PL spectroscopy is a very informative tool of studying the emission properties of semiconductor nanoparticles. Figure 4a shows a typical PL decay profile for the PEI-stabilized CdS QDs. Examples of PL decay profiles for three different time range (0...5, 0...50, 0...500 ns) are given in the Supporting Information (Figure S5). The nonexponential character of PL decays is observed, the fact commonly assigned to energy dispersion of the trapping sites involved and interaction with QD environment.<sup>35,40,41</sup> The decay profiles exhibit emission wavelength dependence, yielding an increase in the average lifetime at longer emission wavelength (Figure 4b). Figure S6 shows that the contribution of the fast components (with the time constants  $\tau_1$ – $\tau_3$ ) into the decay profiles decreases, while that of the slowest exponent (with the time constant  $\tau_4$ ) grows toward the longer PL wavelengths. These results can be an indication of a broad distribution of emitting states for the CdS QDs, as observed previously.<sup>27,35,42–45</sup>

As the wavelength dependences of PL decay time were reported for a wide time range, from the picosecond to nanosecond<sup>42,43</sup> and even to microsecond time range,<sup>37,41</sup> it can be concluded that different mechanisms may contribute to this dependence. On the other hand, a correlation between the nano- and microsecond charge recombination and interfacial transfer channels was observed in our recent study of the broad-band trap-state PL of Cd<sub>1</sub>Zn<sub>1-x</sub>S nanoparticles.<sup>10</sup>

An accordance was also observed between the PL decay and the charging-induced Burstein shift relaxation for the present PEI-stabilized CdS QDs, as discussed below. We therefore may conclude that the emission wavelength dependence of the PL decay time can be a rather general property of the PL emission, but it may be omitted when measured in the “wrong” time scale.

The wavelength dependence of the PL emission was frequently reported for excitonic emission of nanoparticle ensembles<sup>38,46</sup> and explained by the resonant energy transfer from smaller to larger nanoparticles within the ensemble<sup>46</sup> or a size-dependence of the decay rate (due to a finite size dispersion of the nanoparticles in the ensemble).<sup>38</sup> The first explanation is unlikely to apply in the case of CdS-PEI QDs as the absorbing and emitting levels are well separated (by  $\sim 0.6$ – $0.8$  eV), while overlap of the absorption and PL spectra is a necessary condition for the resonant energy transfer. As to the size dependence of the PL decay rate, this hypothesis can be acceptable in our case, as the magnitude of the decay time variation in our case (up to 100%) is comparable to those reported in ref 38. At a small ( $\sim 10\%$ ) size dispersion of the present PEI-stabilized CdS QDs, the large dispersion of the decay time over the emission

wavelength may be explained either by a much stronger dependence of the decay time constants in the size range of  $d < 2$  nm as compared to larger nanoparticles<sup>39</sup> or by alternate effects, for example, energy dispersion of the trap levels.

It has been claimed that the wavelength dependence of the decay time can be only observed for nonexponential PL decay.<sup>39</sup> However, a classical relation of  $t \approx \text{const} \times \lambda_{\text{em}}$  has been reported for the single exponential decaying PL and explained to be a manifestation of the Fermi’s Golden Rule.<sup>47</sup> The rule can manifest itself experimentally as a size dependence of the decay rate,<sup>47–49</sup> especially when the interparticle energy transfer is excluded.<sup>49</sup>

The observed dispersion of the PL decay time over the PL band should not necessary be (only) due to the migration of the photoexcited carriers over the distribution of the trap energies (depths) in the course of their relaxation. It may reflect the relaxation of the carrier over the vibrational levels of the same trap. When the electron gets captured by a deep trap, it loses energy as large as  $\sim 800$  meV that equals  $\sim 400$  optical vibrational quanta of the CdS lattice. Even though the intraband relaxation is usually observed at subps scale, its extension to several picoseconds may not be excluded to explain the shortest PL decay component of the CdS-PEI QDs.

The multiple phonon emission can apparently account for time-spectral dependences. At that, the longer exciton becomes bound to the surface of CdS-PEI QDs, then the higher fraction of excitation energy will be dissipated through vibrational channels, resulting in the observed wavelength dependence of the kinetic PL parameters. The coupling to phonon bath of ligands is also a very plausible way of relaxation of a huge vibrational energy releasing by the photogenerated electron upon trapping.

The longest decay component is of the same order of magnitude as that commonly measured for the trap-state-related PL of CdS nanoparticles,  $\sim 100$  ns.<sup>27,35</sup> Such a slow PL decay at a very high PL efficiency (up to 60–70% at room temperature as discussed below) for the present PEI-stabilized CdS QDs can be explained by a low probability of nonradiative recombination and/or high overlap of the wave functions of conduction band electron ( $e^-_{\text{CB}}$ ) and valence band hole ( $h^+_{\text{VB}}$ ), even when both of them are trapped. This indicates the unique property of the amine groups of PEI to passivate the QD surface.

The small QD diameter can affect the recombination dynamics of the photogenerated charge carriers in two ways. At the stage when the  $e^-_{\text{CB}}-h^+_{\text{VB}}$  pair is just generated and neither of the carriers is trapped, the small localization volume of the pair

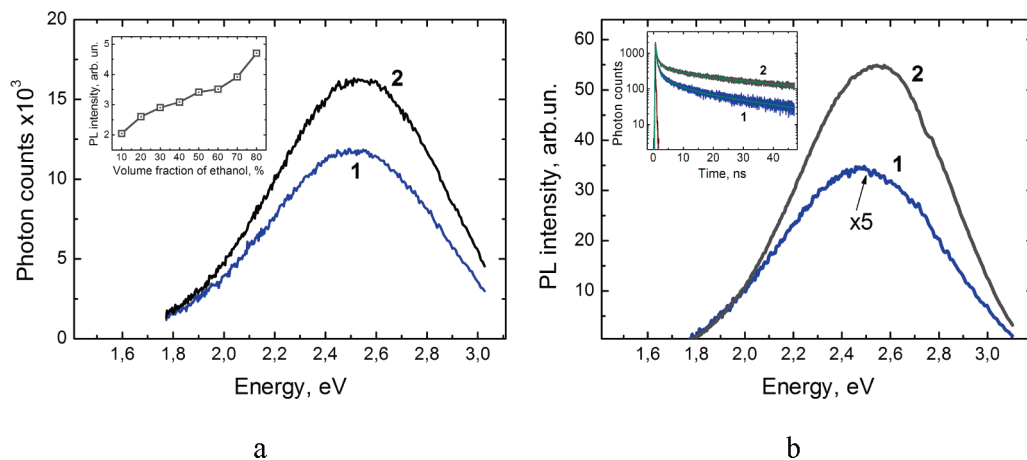


**Figure 5.** (a) Stationary PL spectra of aqueous PEI-stabilized CdS solution diluted by one-half with 0.25% PEI solutions in water (curve 1) and ethanol (curve 2). Inset: PL intensity of PEI-stabilized CdS QDs in water/ethanol mixtures versus volume fraction of alcohol. (b) Stationary PL spectra of aqueous PEI-stabilized CdS colloid (curve 1) and solid film (curve 2) prepared from the colloidal solution by solvent evaporation on a quartz substrate. Curve 1 is multiplied by 5. Inset: PL decay profiles for aqueous PEI-stabilized colloid (curve 1) and a film prepared from the colloid by water evaporation (curve 2).  $[CdS] = 1 \times 10^{-2}$  M, 0.25 wt % PEI.

in the QDs under discussion increases the recombination probability. However, as we did not observe near-bandgap PL even at 77 K (Figure S4a), the direct recombination can obviously not compete with the trapping. Preliminary results showed the lack of excitonic PL features also at temperature as low as 10 K. The trapping of one or both of the carriers at a local surface state(s) seems to be a more rapid process, probably due to the same reason, small nanoparticle size, which provides a strong overlap of the photoexcited carrier wave function with the trapping site. At the same time, the nonradiative recombination channels are very weak in CdS-PEI QDs, as can be concluded from the long-living trap PL with quantum yield as high as 60–70% at room temperature.

In summary, the strongly red-shifted PL band, which lies in the range common for the deep-trap PL widely observed for larger CdS nanoparticles,<sup>10,27,35</sup> unambiguously indicates that at least one of the carriers gets deeply trapped immediately after photoexcitation. However, the strong overlap between the wave functions of the trap and other carrier results in a high-rate radiative recombination channel, which is capable of efficient competition with nonradiative routes.

**PL Discussion – Quantum Yields and Solvent Effect.** Aqueous PEI-stabilized CdS QDs emit visible light in the energy range of 2–3 eV (Figure 1a) with the quantum yield (QY) of up to 12–14% as determined by comparative studies using an alkaline fluorescein solution (QY = 87%<sup>50</sup>) and the solid anthracene (QY = 100%<sup>51</sup>) as reference standards. The PL efficiency increases gradually as the water is replaced by mixed water/ethanol media and the volume alcohol fraction increased, reaching up to 18–20% for 80 vol % ethanol solutions. This result places the PEI-stabilized CdS QDs on line with the apparently best reported white-emitting CdS QDs synthesized in toluene in the presence of oleic acid (17%).<sup>52</sup> For aqueous colloidal CdS solutions, the comparable results have been achieved only using mercapto compounds capable of strong bonding to the QD surface and passivating of the surface states or by a combination of size-selective photocorrosion and passivation by thiols.<sup>21,42,53–55</sup>

The high PL intensity of PEI-stabilized CdS QDs may also be an indication to their crystallinity. In the studies where the amorphous nanoparticles were distinguished from the crystalline ones of the same size, both kinds of nanoparticles revealed similarly broad PL.<sup>30</sup> However, the drastic difference, which,

along with the long-wavelength tail in absorption, can be the criterion of amorphous phase, is believed to be the almost zero Stokes shift between PL and absorption.<sup>30</sup> On the basis of these results, the PEI-stabilized CdS QDs can be considered as crystalline, as they reveal a sharp excitonic absorption feature with a zero background at longer wavelength, as well as a large Stokes shift of the PL band.

The PL intensity was found to be the same for PEI-stabilized CdS QDs prepared in a water/ethanol 50/50 (v/v) mixture, synthesized in water and then diluted in twice with ethanol, or vice versa prepared in 96% ethanol and diluted with water. The facts indicate that the solvent composition is a key factor determining the PL efficiency of CdS QDs rather than some inherent variation of QD properties induced by changes in the synthesis procedure. The same aqueous CdS QDs emit more efficiently when diluted with ethanol than with water with the other conditions unchanged (Figure 5a).

As the solvent was evaporated and a solid film obtained from a colloidal PEI-stabilized solution, the quantum PL efficiency was found to further increase and reach 60–70% irrespectively of starting solvent composition (water, ethanol, or mixed water/ethanol media). At that, the position and shape of PL band remain unchanged (Figure 5b). Upon freezing of aqueous or aqueous-ethanol solutions of CdS-PEI QDs, the quantum yield of emission increases drastically (Figure S4a), reaching almost 100%.

As the inset in Figure 5b shows, the PL decay is faster in aqueous PEI-stabilized CdS colloid than in the film produced from the colloidal solution by solvent evaporation. The time constant sets are  $\tau_1 = 0.14$  ns,  $\tau_2 = 0.80$  ns,  $\tau_3 = 5.2$  ns,  $\tau_4 = 34.5$  ns and  $\tau_1 = 0.16$  ns,  $\tau_2 = 0.91$  ns,  $\tau_3 = 7.1$  ns,  $\tau_4 = 54.4$  ns, respectively, for the solution and the film. Considering the facts, along with the decrease of PL intensity from solid films to water/alcohol mixtures to pure water, we can conclude about the dynamic quenching of emission of PEI-stabilized CdS QDs by water molecules.

The tentative quenching mechanism may be presented as follows. The polyethyleneimine acts as a polyelectrolyte as far as it is dissolved in water (or other protic solvent) capable to dissociate and protonate amino groups of the polymer. According to the pH-metry data (Figure S1a), only 1–2% of protonated

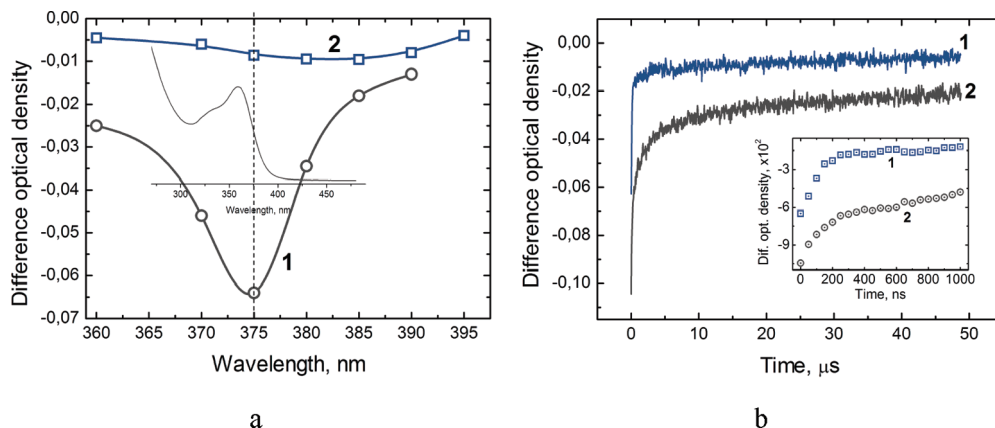


**Figure 6.** (a) Transient bleaching spectra of colloidal PEI-stabilized CdS QDs subjected to laser pulse photoexcitation. The spectra are taken immediately after the pulse extinction ( $t = 0$ , curve 1) and after 200 ns (curve 2). In the background, the stationary absorbance spectrum of the colloidal solution is given. (b) Decay of the transient bleaching of PEI-stabilized 1.8 nm CdS QDs at 370 nm (curve 1) and polyphosphate-stabilized 6–7 nm CdS nanoparticles at 470 nm (curve 2).

$-\text{NH}_2^+$  remain constantly dissociated, indicating that an equilibrium between the protonation/deprotonation processes is established.

As  $\text{Cd}^{2+}$  is introduced into the solution, it forms a complex with amino groups of PEI, shifting the equilibrium toward the deprotonation process. After the formation of CdS QDs, the equilibrium is partially restored, and some portion of surface Cd atoms becomes involved in a competition with water molecules for the amino groups. The surface cadmium(II) sites not bounded with amino groups apparently can serve as the nonradiative recombination centers as is the case for conventional colloidal polymer-stabilized CdS nanoparticles where more than 99% of charge carriers recombine via the nonradiative channels as a rule. The higher is the content of water present in the system, the more efficient become the nonradiative processes, lowering the PL quantum yield. As the protonation/deprotonation of PEI amino groups is of equilibrium character, the water acts as a dynamic PL quencher.

The photochemical processes on the surface of CdS nanoparticles usually contribute to the nonradiative charge decay. With no additional electron acceptor, except for molecular oxygen, present in the system, the photochemical processes usually result in the oxidative photocorrosion of CdS nanoparticles with  $\text{Cd}^{2+}$  and sulfate ions being the final products of the photochemical dissolution of the semiconductor.<sup>21,42,55</sup>

The photochemical stability of PEI-stabilized CdS QDs subjected to the stationary illumination was found to correlate with the PL efficiency, decreasing from the solid films to water/alcohol mixtures to pure water. The solid PEI films incorporating CdS QDs are exceptionally stable in these conditions, displaying no signs of photochemical degradation or PL deterioration even after 2–3 h exposure to the intense flux of 310–390 nm light of a 1000 W mercury lamp. The high photochemical stability of PEI films with CdS QDs coupled with high PL quantum yields (60–70%) make the films an attractive material for light-emitting applications, for example, luminescent paints, solar concentrators, etc.

As the PEI-stabilized CdS QDs contact with water, they lose the photochemical stability and corrode under illumination with the PL quantum yield rapidly falling almost to zero. Surprisingly, opposite to the conventional colloidal polymer-stabilized CdS nanoparticles, which corrode via the oxidative route,<sup>21,42,55</sup> the colloidal PEI-stabilized CdS QDs experience reductive photocorrosion with the formation of  $\text{Cd}^0$  even in the presence of air. The fact of cadmium metal formation was confirmed by

the methylviologen cation-radical  $\text{MV}^{+\cdot}$  formation when  $\text{MV}^{2+}$  was added to the illuminated CdS-PEI solution, due to the reaction  $\text{Cd}^0 + 2\text{MV}^{2+} \rightarrow \text{Cd}^{2+} + 2\text{MV}^{+\cdot}$ . The difference in the mechanism of photochemical corrosion between the present PEI-stabilized CdS QDs and other polymer-capped CdS nanoparticles<sup>56,57</sup> may reflect the different mechanism of primary photoprocesses, in particular, electron–hole recombination, and needs further investigation.

The increased photochemical activity of aqueous PEI-stabilized CdS sols as compared to the solid films is also evidenced by the results of nanosecond laser pulse photolysis. While the solid PEI films gave no transient signals under the laser pulse illumination, aqueous PEI-stabilized CdS QDs manifested a shift of the absorption band edge toward shorter wavelengths when excited by 10 ns laser pulses with  $\lambda = 355$  nm. The shift is observed in a difference spectrum of the colloidal solution as a negative (“bleaching”) nonstationary band with a maximum approximately corresponding to the position of the stationary absorption onset on the half height of the band (Figure 6a, curve 1). The shift (usually referred to as the Burstein shift) is associated with the photoinduced charging of semiconductor nanoparticles and saturation of a fraction of lowest states near the edge of the conduction (valence) band.<sup>53,58,59</sup>

As the charge carriers recombine or get transferred across the semiconductor/electrolyte boundary to electron-accepting (donating) substrates, the transient bleaching band lowers in magnitude (Figure 6b) and shifts to longer wavelength (Figure 6a, curve 2), reflecting the fact that a fraction of larger CdS nanoparticles in the ensemble discharges slower than the rest of nanoparticles.

Figure 6b shows, for the sake of comparison, typical transient bleaching decays for aqueous PEI-stabilized 1.8 nm CdS QDs (curve 1) and conventional polyphosphate-stabilized 5–6 nm CdS nanoparticles (curve 2), registered near the maxima of the corresponding bleaching bands. The photoinduced charging of PEI-stabilized CdS QDs is 6–7 times less efficient, evidently due to the high rate of radiative recombination, and their discharging is much faster as well. As the inset in Figure 6b shows, the major portion of the photoproduct charge decays in the first 200 ns, which is close to the longest time constant of the PL decay profiles, indicating that the radiative recombination is probably the main discharging mechanism in this time range.

**PL Enhancement by  $\text{Cd}^{\text{II}}$ .** The addition of cadmium(II) chloride to the PEI-stabilized CdS QDs results in a PL

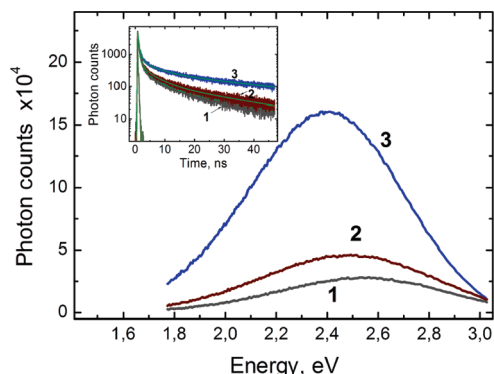


**Figure 7.** Stationary PL spectra and PL decay profiles at 500 nm (inset) for aqueous PEI-stabilized CdS colloid ( $[\text{CdS}] = 1 \times 10^{-2}$  M, 0.25% PEI without additives (curve 1)), and in the presence of  $[\text{Na}_2\text{S}] = 1 \times 10^{-2}$  M (curve 2) and  $[\text{CdCl}_2] = 1 \times 10^{-2}$  M (curve 3).

enhancement and growing of the luminescence lifetime (Figure 7). Excess or addition of  $\text{Cd}^{2+}$  ions to CdS nanoparticles was reported to enhance the intensity of both the excitonic<sup>43,60</sup> and the trap-state emission.<sup>27,42,43,60</sup> Therefore, addition of cadmium ions was assumed to remove the nonradiative recombination states on the nanoparticle surface, most probably lying on the surface sulfur bonds. Moreover, increase of surface termination with cadmium(II), which can coordinate additional amino groups of PEI, is expected to increase the number of radiative deep trap states responsible for the observed deep-trap PL emission.<sup>27</sup> Indeed, in most of the reports on CdS nano- and macrostructures, the deep-trap emission was related to the surface sulfur vacancy, or, in other words, surface Cd atom.<sup>20,27,42,43,60</sup>

Surprisingly, addition of  $\text{S}^{2-}$  anion has a minor effect on the PL intensity. The fact can probably be accounted for by the strong bonding of surface Cd(II) ions in the complex with PEI preventing reconstruction of the surface and formation of nonradiative recombination centers.

## Conclusions

Ultrasmall CdS nanoparticles were synthesized in linear polyethyleneimine solutions in water and water/ethanol mixtures. Colloidal solutions show remarkable aggregative stability at comparatively high CdS concentrations (up to 0.2 M), small nanoparticles size,  $1.8 \pm 0.1$ , as estimated from the position of the first excitonic maximum, and a narrow size distribution of around 10%.

An optimal ratio between the CdS and polymer content as well as between the starting  $\text{Cd}^{2+}$  and  $\text{S}^{2-}$  concentration exists, indicating, along with the above-mentioned unusual properties of CdS-PEI nanoparticles, that a special stabilization mechanism is realized by polyethyleneimine. A complex between  $\text{Cd}^{2+}$  and PEI with an optimal composition of around Cd:N = 1:6 is supposed to be responsible for the formation of both ultrasmall and uniform, stable, and luminescent CdS nanoparticles.

The PEI-stabilized CdS nanoparticles reveal broad-band white-like emission in the range of 2–3 eV and the quantum yield of 12–14% in water, 18–20% in 80 vol % ethanol, and up to 60–70% in solid PEI films obtained by solvent evaporation. Dynamic emission quenching by water is assumed to be accounted for by a competition between Cd atoms on the surface of CdS nanoparticles and water for the  $-\text{NH}-$  groups of the polyelectrolyte, which can passivate surface centers of nonradiative recombination in CdS nanoparticles.

A time-resolved luminescence study revealed strongly non-exponential character of emission decay, consisting of several

(up to four) exponents with the longest time constants in the range of 30–100 ns. The dependence of the emission decay rate on the quantum energy observed in the time-resolved luminescence measurements is assumed to originate from a distribution of both the trap state energies and nanoparticle size.

A study of the photochemical properties of PEI-stabilized CdS nanoparticles both under stationary illumination showed excellent stability of solid PEI films incorporating CdS nanoparticles toward UV illumination and reductive character of the CdS nanoparticle photocorrosion in aqueous solutions. Nonstationary nanosecond laser photolysis of colloidal CdS-PEI nanoparticles showed that the photoexcitation results in the nanoparticle charging and a concomitant Burstein blue shift of the absorption onset. The discharging occurs mainly in 200 ns after the pulse, indicating that the radiative recombination is the principal discharging route.

**Acknowledgment.** We thank Prof. Volodymyr G. Ilyin (Institute of Physical Chemistry, Kyiv, Ukraine) for XRD measurements, and Dr. Aleksey N. Kulak (University of Southampton, UK) for HRTEM measurements. The work is supported by NAS Ukraine and Russian Foundation for Basic Investigations (projects 08-03-90425-Ukr and 32-08-10-Ukr) and the Grant of the President of Ukraine for Young Scientists No. GP/F27/0041.

**Supporting Information Available:** Additional figures. This material is available free of charge via the Internet at <http://pubs.acs.org>.

## References and Notes

- Schreuder, M. A.; Xiao, K.; Ivanov, I. N.; Weiss, S. M.; Rosenthal, S. J. *Nano Lett.* **2010**, *10*, 573–576.
- Park, Y.-S.; Dmytruk, A.; Dmitruk, I.; Kasuya, A.; Takeda, M.; Ohuchi, N.; Okamoto, Y.; Kaji, N.; Tokeshi, M.; Baba, Y. *ACS Nano* **2010**, *4*, 121–128.
- Schreuder, M. A.; McBride, J. R.; Dukes, A. D., III; Sammons, J. A.; Rosenthal, S. J. *J. Phys. Chem. C* **2009**, *113*, 8169–8176.
- Soloviev, V. N.; Eichhofer, A.; Fenske, A. D.; Banin, U. *J. Am. Chem. Soc.* **2001**, *123*, 2354–2364.
- Dai, Q.; Duty, C. E.; Hu, M. Z. *Small* **2010**, *6*, 1577–1588.
- Baker, D. R.; Kamat, P. V. *Langmuir* **2010**, *26*, 11272–11276.
- Li, H.; Shih, W.-H.; Shih, W. Y.; Chen, L.; Tseng, S.-Ja.; Tang, S.-C. *Nanotechnology* **2008**, *19*, 475101.
- Qi, L.; Cölfen, H.; Antonietti, M. *Nano Lett.* **2001**, *1*, 61–65.
- Huang, J.; Sooklal, K.; Murphy, C. J.; Ploehn, H. J. *Chem. Mater.* **1999**, *11*, 3595–3601.
- Stroyuk, A. L.; Dzhagan, V. M.; Zahn, D. R. T.; von Borczyskowski, C. *Theor. Exp. Chem.* **2007**, *43*, 297–305.
- Dzhagan, V. M.; Stroyuk, O. L.; Rayevska, O. E.; Kuchmiy, S. Ya.; Valakh, M. Ya.; Azhniuk, Y. M.; von Borczyskowski, C.; Zahn, D. R. T. *J. Colloid Interface Sci.* **2010**, *345*, 515–523.
- Strekal', N.; Kulakovich, O.; Belyaev, A.; Stsiapura, V.; Maskevich, S. *Opt. Spectrosc.* **2008**, *104*, 50–56.
- Zhelev, Z.; Bakalova, R.; Ohba, H.; Jose, R.; Imai, Y.; Baba, Y. *Anal. Chem.* **2006**, *78*, 321–330.
- Byrne, S. J.; Williams, Y.; Davies, A.; Corr, S. A.; Rakovich, A.; Gunko, Y. K.; Rakovich, Y. P.; Donegan, J. F.; Volkov, Y. *Small* **2007**, *3*, 1152–1156.
- Rogach, A.; Gaponik, N.; Lupton, J. M.; Bertoni, C.; Gallardo, D. E.; Dunn, S.; Li Pira, N.; Paderi, M.; Repetto, P.; Romanov, S. G.; O'Dwyer, C.; Sotomayor Torres, C. M.; Eychmüller, A. *Angew. Chem., Int. Ed.* **2008**, *47*, 6538–6549.
- Mao, J.; Yao, J.-N.; Wang, L.-N.; Liu, W.-S. *J. Colloid Interface Sci.* **2008**, *319*, 353–356.
- Raevskaya, A. E.; Stroyuk, A. L.; Kuchmiy, S. Ya. *Theor. Exp. Chem.* **2003**, *39*, 158–165.
- Yu, W. W.; Qu, L.; Guo, W.; Peng, X. *Chem. Mater.* **2003**, *15*, 2854–2860.
- de Mello Donega, C.; Koole, R. *J. Phys. Chem. C* **2009**, *113*, 6511–6520.
- Vossmeier, T.; Katsikas, L.; Giersig, M.; Popovic, I. G.; Diesner, K.; Chemseddine, A.; Eychmüller, A.; Weller, H. *J. Phys. Chem.* **1994**, *98*, 7665–7771.

- (21) Torimoto, T.; Kontani, H.; Shibutani, Y.; Kuwabata, S.; Sakata, T.; Mori, H.; Yoneyama, H. *J. Phys. Chem. B* **2001**, *105*, 6838–6845.
- (22) Tomasulo, A.; Ramakrishna, M. V. *J. Chem. Phys.* **1996**, *105*, 3612–3618.
- (23) Lippens, P. E.; Lannoo, M. *Phys. Rev. B* **1989**, *39*, 10935–10942.
- (24) Wang, Y.; Herron, N. *Phys. Rev. B* **1990**, *42*, 7253–7255.
- (25) Sarkar, S. K.; Chandrasekharan, N.; Gorer, S.; Hodes, G. *Appl. Phys. Lett.* **2002**, *81*, 5045–5050.
- (26) Herron, N.; Calabrese, J. C.; Farneth, W. E.; Wang, Y. *Science* **1993**, *259*, 1426–1428.
- (27) Spanhel, L.; Haase, M.; Weller, H.; Henglein, A. *J. Am. Chem. Soc.* **1987**, *109*, 5649–5655.
- (28) Kadioglu, S. I.; Yilmaz, L.; Ozbekelge, H. O. *Sep. Sci. Technol.* **2009**, *44*, 2559–2581.
- (29) Epifani, M.; Pellicer, E.; Arbiol, J.; Sergent, N.; Pagnier, T.; Morante, J. R. *Langmuir* **2008**, *24*, 11182–11188.
- (30) Chen, X. B.; Samia, A. C. S.; Lou, Y. B.; Burda, C. *J. Am. Chem. Soc.* **2005**, *127*, 4372–4375.
- (31) Levichev, S.; Rolo, A. G.; Chahboun, A.; Conde, O.; Kovalev, A. I.; Wainstein, D. L.; Gomes, M. J. M. *Phys. Status Solidi A* **2008**, *205*, 1500–1504.
- (32) Vossmeier, T.; Reck, G.; Schulz, B.; Katsikas, L.; Weller, H. *J. Am. Chem. Soc.* **1995**, *117*, 12881–12882.
- (33) Liu, C.; Chung, S.-Y.; Lee, S.; Wess, S.; Neuhauser, D. *J. Chem. Phys.* **2009**, *131*, 174705.
- (34) Nguyen, K. A.; Day, P. N.; Patcher, R. *J. Phys. Chem. C* **2010**, *114*, 16197–16209.
- (35) Chestnoy, N.; Harris, T. D.; Hull, R.; Brus, L. E. *J. Phys. Chem.* **1986**, *90*, 3393.
- (36) Mahdouani, M.; Bourguiga, R.; Jaziri, S. *Physica E* **2008**, *41*, 228.
- (37) Martin, J.; Cichos, F.; Huisken, F.; von Borczyskowski, C. *Nano Lett.* **2008**, *8*, 656–660.
- (38) Atta-Fynn, R.; Bismass, P.; Drabold, D. A. *Phys. Rev. B* **2004**, *69*, 245204.
- (39) Yu, M.; Fernando, G. W.; Li, R.; Papadimitrakopoulos, F.; Shi, N.; Ramprasad, R. *Appl. Phys. Lett.* **2006**, *88*, 231910.
- (40) Jones, M.; Lo, S. S.; Scholes, G. D. *Proc. Natl. Acad. Sci. U.S.A.* **2009**, *106*, 3011–3016.
- (41) Jones, M.; Lo, S. S.; Scholes, G. D. *J. Phys. Chem. C* **2009**, *113*, 18632–18642.
- (42) Harruff, B. A.; Bunker, C. E. *Langmuir* **2003**, *19*, 893–897.
- (43) Uchihara, T.; Kato, H.; Miyagi, E. *J. Photochem. Photobiol., A* **2006**, *181*, 86–93.
- (44) Kobitski, A. Yu.; Zhuravlev, K. S.; Wagner, H. P.; Zahn, D. R. T. *Phys. Rev. B* **2001**, *63*, 115423.
- (45) Baker, D. R.; Kamat, P. V. *Langmuir* **2010**, *26*, 11272–11276.
- (46) Crooker, S. A.; Hollingsworth, J. A.; Tretiak, S.; Klimov, V. I. *Phys. Rev. Lett.* **2002**, *89*, 186802.
- (47) Aharoni, A.; Oron, D.; Banin, U.; Rabani, E.; Jortner, J. *Phys. Rev. Lett.* **2008**, *100*, 057404.
- (48) Wu, F.; Zhang, J. Z.; Kho, R.; Mehra, R. K. *Chem. Phys. Lett.* **2000**, *330*, 237–242.
- (49) Hassan, M. L.; Ali, A. F. *J. Cryst. Growth* **2008**, *310*, 5252–5258.
- (50) Grabolle, M.; Spieles, M.; Lesnyak, V.; Gaponik, N.; Eychmueller, A.; Resch-Genger, U. *Anal. Chem.* **2009**, *81*, 6285–6294.
- (51) Pringsheim, P.; Vogel, M. *Luminescence of Liquids and Solids and Its Practical Application*; Interscience Publishers: New York, 1946.
- (52) Sapra, S.; Mayilo, S.; Klar, T. A.; Rogach, A. L.; Feldmann, J. *Adv. Mater.* **2007**, *19*, 569–572.
- (53) Yang, B.; Schneeloch, J. E.; Pan, Z.; Furis, M.; Achermann, M. *Phys. Rev. B* **2010**, *81*, 073401.
- (54) Kuwabata, S.; Ueda-Sarson, K.; Torimoto, T. *Chem. Lett.* **2004**, *33*, 1344–1345.
- (55) Matsumoto, H.; Sakata, T.; Mori, H.; Yoneyama, H. *J. Phys. Chem.* **1996**, *100*, 13781–13785.
- (56) Stroyuk, O. L.; Rayevska, O. Ye.; Kozytskiy, A. V.; Kuchmiy, S. Ya. *J. Photochem. Photobiol., A* **2010**, *210*, 209–214.
- (57) Stroyuk, O. L.; Sobran, I. V.; Korzhak, G. V.; Rayevska, O. Ye.; Kuchmiy, S. Ya. *Colloid Polym. Sci.* **2008**, *286*, 489–498.
- (58) Liu, C.; Bard, A. J. *J. Phys. Chem.* **1989**, *93*, 3232–3237.
- (59) Stroyuk, O. L.; Dzhagan, V. M.; Shvalagin, V. V.; Kuchmiy, S. Ya. *J. Phys. Chem. C* **2010**, *114*, 220–225.
- (60) Zhang, J. Z. *J. Phys. Chem. B* **2000**, *104*, 7239–7253.

JP108561U